Estimation of Dynamic Stability Derivatives of a Generic Aircraft

Stefan Schmidt[1] **and Daniel M. Newman**[2]

[1]Defence Science and Technology Organisation
Fishermans Bend, Victoria, 3207 AUSTRALIA

[2]Quantitative Aeronautics Pty Ltd
Glebe, New South Wales, 2037 AUSTRALIA

Abstract

In this paper dynamic stability derivatives of an aircraft subjected to periodic pitch oscillations are calculated from the resulting time histories of forces and moments obtained by numerical simulation. These values depend on the quality of the simulation data, angle-of-attack, the amplitude of the forced oscillation as well as the user selection for the post-processing routine. The results show reasonable agreement with experimental reference data and can be regarded as proof of concept. Non linearity in the vehicle response can be limited by a reduction of the forcing amplitude.

Introduction

Computational fluid dynamics (CFD) has been a major tool for the design of air vehicles for some time now. Beside ensuring the vehicles performance within its operational limits, CFD is also applied to off-design scenarios such as high-lift or even stall. However, these design points are calculated mainly using steady-state approaches. These disregard dynamic effects such as unsteady manoeuvres of an aircraft in which the flow history plays an important role. In order to determine the stability of an aircraft under a set of conditions (Re, Ma, angle-of-attack α, angle-of-sideslip β) dynamic stability derivatives, also known as aerodynamic transfer functions, or rate derivatives need to be considered. In the past, the most common means of determining derivatives was wind tunnel testing. First numerical attempts were made with doublet-lattice methods [7]. Later, these values could be determined from the Digital Data Compendium (DATCOM [10]). However, these values are only valid for traditional fixed-wing aircraft shapes with cylindrical fuselages, which have vertical and horizontal stabilizers, but would fail for aircraft with highly swept or delta wings and also cannot account for inlets, twin-tails or canards.

Table 1: SDM: Model Dimensions.

Length	0.943 m
Span	0.609 m
MAC	0.229 m
Wing Area	0.117 m^2
Fuselage Diameter	0.135 m

Geometry

In this study the Standard Dynamics Model (SDM [9], figure 1) is used as a generic aircraft. The shape resembles that of an F-16 with its cylindrical fuselage and simple shaped wings and stabilizers, allowing for relatively easy manufacturing of the model for wind tunnel testing and computational modeling. Due to geometrical symmetry, only the half model is considered. The model dimensions reference values used to normalize the forces and moments match those found in the experimental study [1] and are shown in table 1.
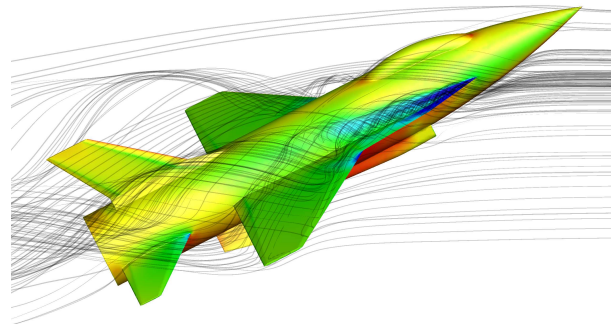

Figure 1: Standard Dynamics Model at $\alpha = 30°$.

Numerical Method

The full Reynolds-Averaged Navier–Stokes equations are solved using a density-based finite-volume method of second order in space and time called Cobalt [2]. It is based on a a compact first-order accurate Riemann solver, combining an approximate Riemann method of Colella and a Newton procedure of Gottlieb and Groth. The accurate estimation of gradients requires special care in aerodynamic CFD codes. In Cobalt, a least-square technique based on a QR decomposition ensures the values stay within limits and does not produce any nonphysical values. The linearized equation system is solved with a Gauss-Seidel algorithm found to be better than a Jacobi method. Turbulence is modeled using the two-equation shear-stress transport (SST) model of Menter [5].
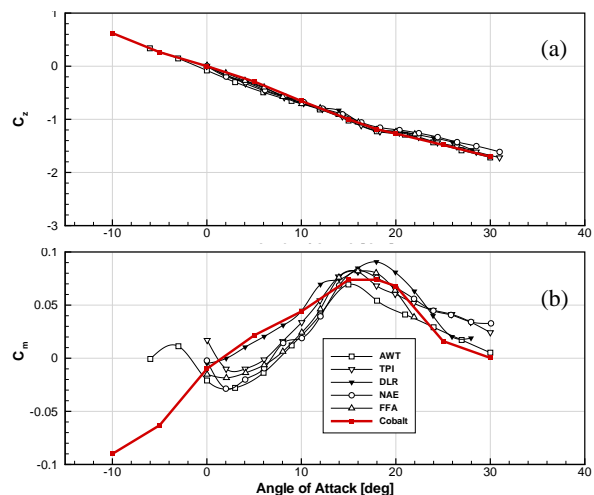

Figure 2: SDM: steady-state coefficient of lift (a) and pitching moment (b); AWT - Ankara Wind Tunnel, Turkey [1], TPI - Politechnico di Turino, Italy [3], DLR (Germany), NAE (Canada) and FFA (Sweden).

Steady-State Results

Figure 2 shows the normal force and pitching moment coefficients for an α-sweep. While the predicted normal force is very close to the measurements, there is some scatter in the pitching moment due to different wind tunnel blockages and model mounts [3]. Remaining differences can be attributed to low mesh resolution around the base and off-surface areas, which was kept intentionally limited. These are also present in the Cz data, but are a smaller fraction of the total coefficient. The CFD results fall in that scatter and form the baseline for the following dynamic simulations.

Dynamic Results

The dynamic runs at $\alpha = 0°, 10°, 20°, 30°$ were started from the converged steady-state solution at the same angle-of-attack. The model underwent periodical pitch oscillations at f=2Hz (as in [1]) with an amplitude of $\alpha_A = 1°$ and $5°$. Although the latter value is much too high to approximate the linear aerodynamics it was included for comparison with a different aircraft configuration not shown here. A total simulation time of $t_S = 2s$ covered four full oscillation cycles at a time step of $\Delta t = 10^{-3}s$. Unsteady RANS (URANS) was used for these simulations despite the well-known limitations of that approach regarding the ability to resolve parts of the turbulent spectrum directly [4]. As long as the imposed frequencies compared to dominant eddy-turnover times are small enough, this approach can be justified.
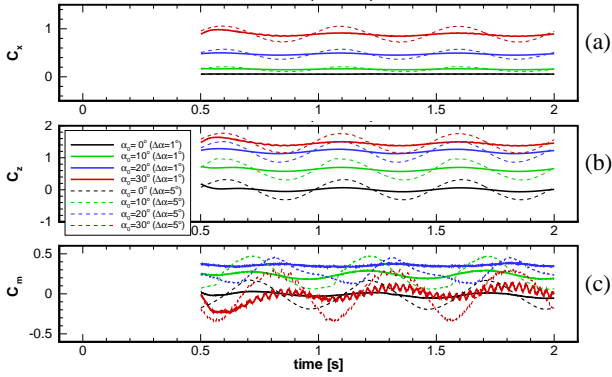
Figure 3: SDM: time history of pitch oscillation: axial force (a), normal force (b) and pitching moment (c).

The time histories for axial and normal force and the pitching moment are shown in figure 3 for two forcing amplitudes $\alpha_A = 1°$ and $5°$. Due to scaling the results for $\alpha_A = 1°$ appear to be fairly linear. The forces are linear up to $\alpha_A = 5°$, whereas the pitching moment (cf. figure 3c) shows a sinusoidal response. However, at high angles-of-attack, superimposed high-frequency noise can be seen. This is caused by variational vortex-shedding patterns originating at the leading-edge extension. The results with respect to angle-of-attack (cf. figure 4a-c) show that behaviour more clearly. The axial force response as well as the normal force reveal the existence of hysteresis loops, which arise because of the phase difference of the stiffness and damping contributions. For Cz, the stiffness terms predominate, so the hysteresis loops are quite flat, but increase with angle of attack (figure 4a). For Cm, however, the stiffness terms are much less dominant and so the hysteresis becomes more circle-like (figure 4c). While the dynamic normal force coefficients remain close to their static values, the pitching moment coefficient diverts from these values quite significantly, particularly at intermediate angle-of-attacks. The axial force steadily increases and suggests that with increasing α, some flow features such as flow separation and vortex breakdown are not properly resolved.
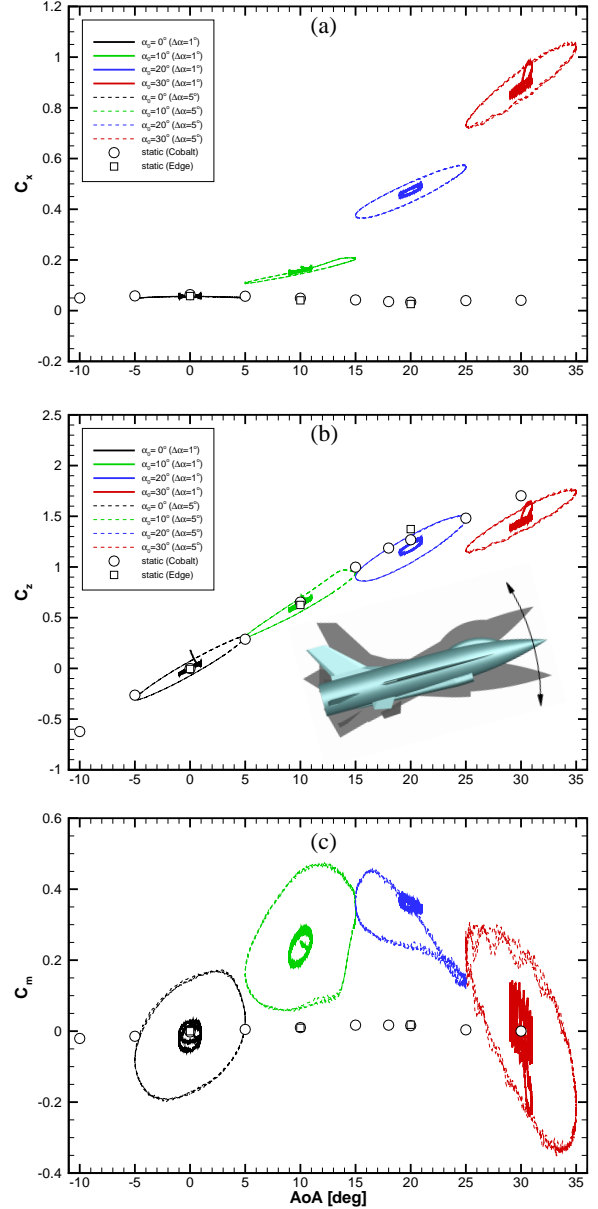
Figure 4: SDM: phase diagram of pitch oscillation: axial force (a), normal force (b) and pitching moment (c) at $\alpha = 0°, 10°, 20°, 30°$.

Dynamic Derivatives

Theory

The rate derivatives can be directly computed from the time histories of the forces and moments in a post-processing step leaving the bulk of the task to the generation of the database. The method to determine these derivatives follows that described in Newman [6] and the main parts as well as limitations of the current approach are briefly outlined here.

In a harmonic pitching motion, the angle-of-attack α and pitch rate q are

$$\alpha(t) = \alpha_0 + \alpha_A \cos(\omega t) \qquad (1)$$
$$\Rightarrow \quad \dot{\alpha}(t) = -\alpha_A \omega \sin(\omega t) \qquad (2)$$
$$q(t) = -\alpha_A \omega \sin(\omega t) \qquad (3)$$

During one pitch cycle, $\dot{\alpha}$ and q are equal and consequently

aerodynamic forces and moments as well as their higher derivatives cannot be linked to either value and therefore only the combined effect of both can be calculated. Accounting for angle-of-attack and pitch-rate variations the time-dependent pitching moment can be written as

$$Cm(t) = Cm_\alpha \, \alpha(t) + Cm_{\dot\alpha} \, \dot\alpha(t) \frac{c}{2U} + Cm_{\ddot\alpha} \, \ddot\alpha(t) \frac{c^2}{4U^2} + ...$$
$$+ Cm_q \, q(t) \frac{c}{2U} + Cm_{\dot q} \, \dot q(t) \frac{c^2}{4U^2} + ... \qquad (4)$$

with

$$Cm_\alpha = \frac{\partial Cm}{\partial \alpha} \ , \quad Cm_{\dot\alpha} = \frac{\partial Cm}{\partial \frac{\dot\alpha c}{2U}} \ , \quad Cm_{\ddot\alpha} = \frac{\partial Cm}{\partial \frac{\ddot\alpha c^2}{4U^2}} \ ,$$

$$Cm_q = \frac{\partial Cm}{\partial \frac{qc}{2U}} \ , \quad Cm_{\dot q} = \frac{\partial Cm}{\partial \frac{\dot q c^2}{4U^2}} \ . \qquad (5)$$

Small perturbation theory demands that only terms up to first-order (linear) will be considered ($\ddot\alpha, \dot q \to 0$) and substitution of the remaining terms with equations 1 and 3 and introducing the reduced frequency $k = \omega c/(2U)$ leads to

$$Cm(t) = Cm_\alpha \, \alpha + Cm_{\dot\alpha} \, \frac{\dot\alpha k}{\omega} + Cm_q \, \frac{qk}{\omega}$$
$$\Rightarrow \quad = Cm_\alpha \, \alpha_A \cos(\omega t)$$
$$- \left(Cm_{\dot\alpha} + Cm_q \right) k \, \alpha_A \sin(\omega t) \qquad (6)$$

This is the analytical form of the pitching moment coefficient written in terms of dynamic derivatives. After the simulation is carried out and the vehicle response has been recorded, the information in figure 3 needs to be analyzed. As it may also contain a phase angle δ in relation to the forcing function (eqn.1), the pitching moment coefficient is kept as general as possible and can be evaluated to

$$Cm(t) = Cm_A \cos(\omega t - \delta) \ .$$

Applying simple trigonometric laws we end up with

$$Cm(t) = Cm_A \cos(\omega t) \cos\delta + Cm_A \sin(\omega t) \sin\delta \ , \qquad (7)$$

which contains an amplitude Cm_A and phase angle δ to be determined by a curve-fitting process. This could be done automatically, but currently it requires the user to select the data range and therefore the outcome may vary. Comparing equations 6 and 7 allow us to identify the two unknown derivatives referred to as pitching moment coefficient 'stiffness' and 'damping':

$$Cm_\alpha = \frac{Cm_A}{\alpha_A} \cos\delta \ , \qquad (8)$$

$$Cm_{\dot\alpha} + Cm_q = -\frac{Cm_A}{(k\,\alpha_A)} \sin\delta \ . \qquad (9)$$

The method described here, can be applied to all forces and moments (Cx, Cz, Cm) in the same fashion. It is valid for single-frequency pitch oscillation and therefore cannot be used for other manoeuvres such as roll, yaw or combinations of any. The combined damping terms $Cm_{\dot\alpha} + Cm_q$ can be separated by applying a harmonic plunging motion to the aircraft ($q \equiv 0$) and using a modified post-processing routine to calculate $Cm_{\dot\alpha}$. The method described here as well as more sophisticated methods to determine dynamic derivatives, which are also able to account for non-linear content in the vehicle response, can be found in Rohlf et al. [8].
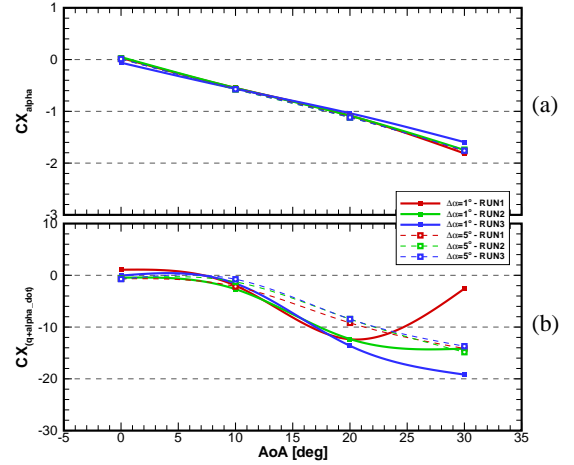

Figure 5: SDM: axial force stiffness and damping

Results

Figures 5-7 show the results for the dynamic derivatives for the axial and normal force coefficient as well as the pitching moment coefficient. For each forcing amplitude α_A these graphs show three sets of results. They refer to different selection windows used in the curve-fitting process and are denoted as RUN1..3. The axial force stiffness almost linearly increases as indicated by figure 4a and its damping curve (figure 4b) starts from zero values (at $\alpha = 0°$) and has its largest descent between $10° - 20°$ to level off at the largest angle-of-attack ($\alpha = 30°$). The change of the forcing amplitude has no effect on the stiffness and only marginally affects the damping, in which the set of curves untangle and show different results for $\alpha_A = 5°$. This is attributed to the choice of the data window, forming the basis for the curve fit. The stronger non-linear content in the vehicle response at high angles-of-attack violates the linear theory-assumption made in the design of the procedure to calculate the derivatives. It therefore omits the information contained in the non-linearity and the results may lack that contribution. However, these possible errors become apparent as multiple solutions in the graphs. At lower forcing amplitudes, however, all solutions collapse and the data range has no effect on the outcome, which was the prime reason for choosing lower forcing amplitudes.
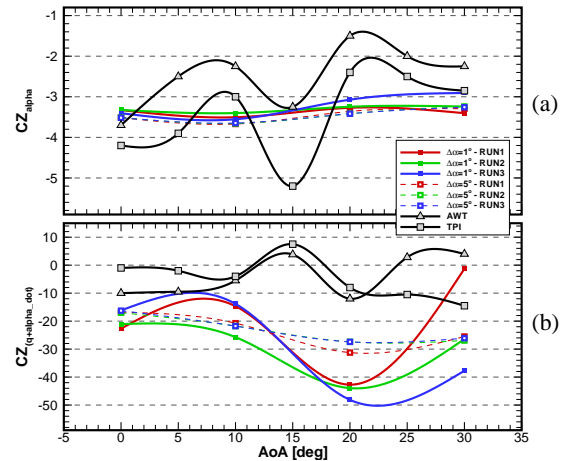

Figure 6: SDM: normal force stiffness and damping

The stiffness and damping for the normal force Cz is shown in figure 6. In addition to the present data, results from two independent experiments (AWT and TPI, taken from [1]) are added

for comparison. These data agree qualitatively and show distinct minima in stiffness and damping at $\alpha = 15°$. None of the CFD results show that behaviour. They remain at lower values without being affected by either the forcing amplitude or the data window. As for the damping: there is some scatter at larger forcing for all angles-of-attack, whereas again the low-forcing results tend towards a single solution. Although the dynamic normal force coefficients stay in proximity to the steady state counterparts (figure 4), the mismatch of CFD and experiments for the stiffness of that force coefficient is due to the different slope angles of the hysteresis loop, which directly affect the stiffness derivative Cz_α.
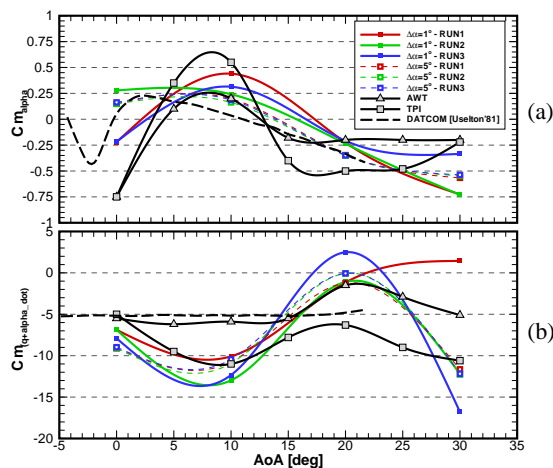

Figure 7: SDM: pitching moment stiffness and damping

The pitching moment coefficient stiffness and damping (shown in figure 7a) show reasonably good agreement for the α-range investigated. While the numerical stiffness results reveal a local maximum at $\alpha = 5 - 10°$ ending up in a linear decline, both experiments also have the peak at $\alpha = 5 - 10°$, but then level-off to almost constant values past $\alpha = 15°$. On the other hand, the pitch-damping (figure 7b) based on the CFD data remarkably captures the trends and values of the experiment, despite some differences in these data sets (AWT/TPI). In addition, DATCOM data (taken from [9]) is added for reference and only show qualitative agreement without detecting any angular dependency in the pitch damping.

At first glance, the rather good prediction of the pitching moment derivatives in comparison to the normal force derivatives appears to be surprising, considering the gross deviations of the dynamic forces and moment from the static one in figure 4. However, the curve-fitting procedure is affected by errors in the contribution of the forces and moments. For the normal force coefficient Cz, the stiffness overwhelms the damping contribution and the uncertainty of the curve-fit is more biased towards the damping (cf. figure 6). For the pitching moment coefficient on the other hand, the stiffness and damping are of the same order, resulting in a more balanced error distribution for the curve fit and an apparent better agreement with reference data (cf. figure 7).

Conclusions

This paper documents the capability to predict dynamic derivatives using CFD-based methods using RANS. The aircraft model was kept fairly coarse to aid computing times. Two sets of pitch oscillation cases with different forcing amplitudes were run. Longitudinal stability derivatives were estimated and compared to experimentally obtained values. The results compare more favourably in the linear range (at low α) than for higher

angles-of-attack, where non-linear effects limit the validity of the method. In this case, vortex shedding is the most dominant effect and creates a wide range of turbulent scales, which directly affect the load distribution on the aircraft and the pitching moment in particular. As a consequence, the described procedure is more susceptible to the selection of the user window used for the curve fit, which determines the derivatives. The non-linear content can be reduced by decreasing the forcing amplitude to lower angles.

The same procedure has been used for harmonic yaw oscillation, but others or even combined manoeuvres can be easily implemented – just follow the steps described and substitute equations 1 and 3 with other forcing vectors and consider that other derivatives come into play, which are also very important for stability and control analysis.

References

[1] Altun, M. and Iyigün, I., Dynamic Stability Derivatives of a Manuevering Combat Aircraft Model, *Journal of Aeronautics and Space Technologies*, **1**, 2004, 19–27.

[2] Grismer, M., Strang, W., Tomaro, R. and Witzeman, F., Cobalt: A parallel, implicit, unstructured euler/navier–stokes solver, *Adv. Eng. Software*, **29**, 1998, 365–373.

[3] Guglieri, G. and Quagliotti, F. B., Dynamic stability derivatives evaluation in a low-speed wind tunnel, *J. Aircraft*, **30**, 1993, 421–423.

[4] Lübcke, H., Schmidt, S., Rung, T. and Thiele, F., Comparison of LES and RANS in bluff-body flows, *J. Wind Eng. Ind. Aerodyn.*, **89**, 2001, 1471–1485.

[5] Menter, F., Two-Equation Eddy-Viscosity Turbulence Model for Engineering Applications, *AIAA Journal*, **32**, 1994, 1598–1605.

[6] Newman, D.M., Measurement of Water Tunnel Model Dynamic Derivatives using a Force Balance Capable of Rotational Oscillation, Contractor Report 2005.003, V0.20, Quantitative Aeronautics, 2006.

[7] Rodden, W. and Giesing, J., Application of Oscillatory Aerodynamic Theory to Estimation of Stability Derivatives, *J. Aircraft*, **7**, 1970, 272–275.

[8] Rohlf, D., Schmidt, S. and Irving, J., SACCON Stability and Control Analyses Applying System Identification Techniques, *28th AIAA Applied Aerodynamics Conference, Chicago, IL, USA*.

[9] Uselton, B.L., A description of the Standard Dynamic Model (SDM), Technical report, 56th STA Meeting, MIT, Cambridge, Massachusetts, USA, 1981.

[10] Williams, John E. and Vukelich, Steven R., The USAF Stability and Control Digital DATCOM, *Technical Report, AFFDL-TR-79-3032, Volumes I-III*.